Transport Property Requirements for Flow Battery Separators

Robert Darling,[a,b,*,z] Kevin Gallagher,[a,c,*] Wei Xie,[a,b] Liang Su,[a,d] and Fikile Brushett[a,d,*]

[a]*Joint Center for Energy Storage Research*
[b]*United Technologies Research Center, East Hartford, Connecticut 06108, USA*
[c]*Chemical Sciences and Engineering Division, Argonne National Laboratory, Lemont, Illinois 60439, USA*
[d]*Department of Chemical Engineering, Massachusetts Institute of Technology, Cambridge, Massachusetts 02139, USA*

Flow batteries are a promising technology for storing and discharging megawatt hours of electrical energy on the time scale of hours. The separator between the positive and negative electrodes strongly affects technical and economic performance. However, requirements for separators have not been reported in a general manner that enables quantitative evaluation of new systems such as nonaqueous flow batteries. This gap is addressed by deriving specifications for transport properties that are chemistry agnostic and align with aggressive capital cost targets. Three key transport characteristics are identified: area-specific resistance R_Ω, crossover current density i_x, and the coupling between crossover and capacity loss Ψ. Suggested maximum area-specific resistances are 0.29 and 2.3 $\Omega \cdot cm^2$ for aqueous and nonaqueous batteries, respectively. Allowable crossover rates are derived by considering the possible fates of active molecules that cross the separator and the coupling between Coulombic efficiency (CE) and capacity decline. The CE must exceed 99.992% when active species are unstable at the opposing electrode, while a CE of 97% can be tolerated when active molecules can be recovered from the opposing electrode. The contributions of diffusion, migration, and convection are discussed, quantified, and related to the physical properties of the separator and the active materials.

Energy storage can mitigate electrical transmission bottlenecks and provide ancillary services in addition to supplying stable and continuous power when coupled to inherently variable renewable energy sources or placed in remote regions or districts with unreliable grids.[1–4] Redox flow batteries (RFBs) are a class of electrochemical devices that are suitable for storing energy for multiple hours as described in several recent review articles.[3,5–8] In a flow battery, the reactants or active materials are stored in external tanks separate from the reactor, enabling independent scaling of energy and power. This segregation permits cost effective implementation of electrochemical couples with low energy density. The reactants are commonly ions dissolved in an electrolyte at concentrations near 1 mol/L. A conventional battery like lead acid or lithium ion utilizing active materials with such low volumetric capacity would incur tremendous cost, mass, and volume penalties because the amount of inactive material, principally current collectors and separators, scales with volumetric capacity in enclosed architectures.[9] Appropriately designed flow batteries optimize the power density of the reactor, consequently minimizing the contributions of separators and current collectors to total system cost.

The primary functions of a separator are to prevent shorting of the electrodes while allowing ionic charge carriers to move freely.[10] Any material that fulfills these basic functions is referred to as a separator in this work. The term membrane is reserved for a separator that selectively favors transport of a desired charge carrier, like protons, and thwarts transport of other components like redox molecules and solvents. The complexity of separators used in electrochemical storage and conversion devices varies dramatically. Early in the development of these devices, separators made from simple cloth or even wood were common.[10] Today, sophisticated engineered materials are routinely used and research and development continues at a fast pace as ever more functionality is demanded. Some flow batteries rely on nanoporous (i.e. <100 nm pores) polyolefin separators, while others use ion-exchange membranes like DuPont's Nafion. Despite being expensive, ion-exchange membranes like Nafion are favored in flow batteries because high hydraulic resistance and proton conductivity are desired in addition to electrical isolation and chemical stability.

The low production volumes needed to support existing industries including Chlor-alkali, electrolysis, and fuel cells have resulted in pricing levels on par with specialty chemicals.[11] Techno-economic modeling for PEFCs projects that a substantial increase in production would result in an order-of-magnitude reduction in price.[12–14] Thus, reliance on membranes like Nafion should not present an insurmountable barrier to achieving future cost goals. However, moderate-to-high specific cost will be required in the mid-term to cover costs associated with scaling production if market demand rises.

Recent research into separators for vanadium RFBs has been reviewed by Schwenzer et al.[15] The publications cover a broad range of materials including cation-exchange fluorocarbons, cation-exchange hydrocarbons, anion-exchange polymers, amphoteric polymers, and nonionic separators. Any new separator intended to supplant Nafion in aqueous RFBs must demonstrate a significant improvement in at least one key metric, like resistance or crossover, without sacrificing other critical aspects of performance. Porous separators with low hydraulic resistance and no selectivity are also employed in RFBs. The operative philosophy is to use inexpensive materials at the expense of technical performance and this approach can only be implemented when all active species are stable at both electrodes. This methodology has been applied to aqueous iron-chrome batteries where both reactants are added to both electrolytes during commissioning to minimize capacity loss. Low Coulombic efficiency (CE) is an unavoidable side effect of this approach.

Shin et al. recently reviewed the status of separators for nonaqueous flow batteries.[16] Nonaqueous flow batteries may be regarded as a burgeoning concept at a considerably lower technology readiness than their aqueous counterparts. Anion-exchange membranes have been utilized to a great extent in nonaqueous cells because the majority of redox molecules have been positively charged. Nafion and similar cation-exchange membranes are expected to receive more interest as concerns about chemical costs compel research and development of negatively charged active species to avoid expensive counter-ions like PF_6^-. Doyle et al. systematically examined the behavior of perfluoro-sulfonic acid cation-exchange polymers in contact with a broad range of solvents in two papers focused on possible use in Li-ion batteries.[17,18] These reports provide foundational information about the behavior of cation-exchange membranes in contact with nonaqueous solvents that might be used in future RFBs.

*Electrochemical Society Active Member.
[z]E-mail: darlinrm@utrc.utc.com

Mathematical Analysis

The purpose of this analysis is to derive electrochemical performance requirements that encompass separators for aqueous and nonaqueous flow batteries. Analyses of mechanical, manufacturing, stability, and compatibility demands are beyond the scope of this work. The key attributes examined are area-specific resistance (ASR) and parasitic crossover of active species. ASR targets are determined as a function of open-circuit voltage (OCV) using a Monte Carlo analysis that features an aggressive capital cost goal of $120/kWh and optimistic future component costs. Distinct targets are proffered for aqueous and nonaqueous environments. Allowable crossover currents are derived that consider both capacity loss and energy efficiency (EE). A set of equations describing transport of active species across the separator is presented and the consequences of different modes of transport on cell operation are discussed. The various terms in the transport equations are examined and classified as first or second order. Finally, separator requirements are presented in the form of measurable transport phenomena. Exemplary results for aqueous systems are used to illustrate and quantify phenomena where instructive. A companion manuscript detailing the status of membranes and separators for nonaqueous RFBs in light of the specifications determined here is planned.[19]

Area-specific resistance.— The capital cost of a flow battery may be expressed as the sum of reactor, chemical, auxiliary equipment, and other costs. The last category includes depreciation, labor, overhead, and margin. Installation costs are not considered in this work due to their inherently variable and site-specific nature. The contribution made by the reactor is:[9]

$$p_r = \frac{\sum c_i \cdot \sum R_i}{\varepsilon_{sys,d} U^2 \varepsilon_{v,d}(1 - \varepsilon_{v,d})\, t_d} \rightarrow$$

$$\sum R_i = \frac{p_r \varepsilon_{sys,d} U^2 \varepsilon_{v,d}(1 - \varepsilon_{v,d})\, t_d}{\sum c_i} \qquad [1]$$

p_r is the capital cost of the reactor in $/kWh, c_i is the cost of component i per unit area in $/m^2, R_i is the ASR of component i in $\Omega \cdot$ m^2 (or more commonly $\Omega \cdot$ cm^2), $\varepsilon_{sys,d}$ is the efficiency of the system supporting the battery when it discharges, U is the open-circuit voltage in V, $\varepsilon_{v,d}$ is the average voltage efficiency (VE) during discharge, and t_d is the discharge time in h. We introduce $R_\Omega = \Sigma R_i$ and the resistance of the separator or membrane, R_m, to simplify notation. In our previous analysis, we allocated $60/kWh to the sum of the reactor and chemical costs in order to achieve a system cost of $120/kWh (see Figure 3 in Reference 9).

A Monte Carlo algorithm where values of p_r, U and $\{c_i\}$ were randomly selected from triangular probability distributions and introduced into Equation 1 was used to define distinct ASR requirements for aqueous and nonaqueous batteries. The remaining parameters, $\varepsilon_{sys,d}$, $\varepsilon_{v,d}$ and t_d were treated as invariant specifications. The ASR was calculated for 5000 combinations of parameters. Table I shows the minimum, mode, and maximum for each probability distribution.

Mean values, equal to one third of the sum of the minimum, mode, and maximum, are provided in the final column. The calculated nonaqueous ASR can be approximately corrected, for example, to a particular OCV, by multiplying by $(U/3.5)^2$, where 3.5 V is the mean OCV for nonaqueous flow batteries.

The reactor cost, p_r, was found by fitting the ratio of reactor cost to the sum of reactor plus chemical costs estimated by Darling et al.[9] to a triangular distribution function and multiplying the results by $60/kWh. The chemical or energy cost in a nonaqueous flow battery is approximately 2X to 9X more than the reactor or power cost according to the inputs in Table I. On average the reactor comprises 23% of the $60/kWh allocated to the sum of reactor plus chemicals. Identical values of p_r were used for aqueous and nonaqueous batteries to facilitate comparison. Separator costs were taken from a logarithmic curve fit to a projection done for thin ion-exchange membranes for PEFCs for automobiles; the relevant production volumes are shown in parentheses in the fifth row of Table I.[12] The lower volumes are incompatible with the goal of storing 1% of global electricity production, but they serve to temper the optimism of the predictions and help to bridge the gap to product introduction. For the sake of comparison, reverse osmosis membranes range from 20 to 40 $/m^2 [20] and polyolefin separators for lithium-ion batteries cost about 1 $/m^2.[21] The remaining component costs are taken from our previous work and are intended to apply to a future state characterized by high production.[9] The Monte-Carlo algorithm returns a truncated normal distribution for the ASR with a mean of 3.5 $\Omega \cdot$ cm^2 and a standard deviation of 1.2 $\Omega \cdot$ cm^2 for nonaqueous batteries. The requirement is set at the mean minus one standard deviation, 2.3 $\Omega \cdot$ cm^2, which covers 84.1% of the simulations. The target ASR for nonaqueous batteries is $\sim$10X larger than the best results reported for aqueous systems. For example, Cho et al. reported an ASR of 0.23 $\Omega \cdot$ cm^2 for an aqueous H$_2$-Br cell with a 15 μm reinforced membrane.[22] The Monte-Carlo simulations gave a mean of 0.45 $\Omega \cdot$ cm^2 with a standard deviation of 0.16 $\Omega \cdot$ cm^2, yielding a target of 0.29 $\Omega \cdot$ cm^2 for aqueous batteries. The discharging current densities that coincide with the ASR targets at the prescribed OCVs and VE are 130 and 360 mA/cm^2 for nonaqueous and aqueous, respectively.

Figure 1a shows how required resistance varies with separator cost. Curves are shown for five open-circuit voltages. The remaining parameters were randomly selected from the probability distributions in Table I. Separator cost was selected as the independent variable because realistic estimates vary over a wide range. The two lowest OCVs, 1 V and 1.5 V, are characteristic of aqueous flow batteries, while the larger OCVs are characteristic of nonaqueous systems. The maximum allowable ASR is a strongly decreasing function of membrane cost. The figure and inset indicate that a nonaqueous flow battery at 3.5 V can tolerate an ASR that is roughly 5–6X larger than its aqueous counterpart at 1.5 V because of the benefits associated with higher voltage. Figure 1b shows the dicharging current densities that are consistent with the ASRs in Figure 1a at a VE of 91.6%. The figure shows current density to be a linear function of membrane cost with a slope and intercept that both increase as OCV decreases.

The ASR of a separator depends on both thickness and the inherent conductivity of the material. Figure 2 depicts the trade between

Table I. Parameters for Triangular Probability Distribution Functions.

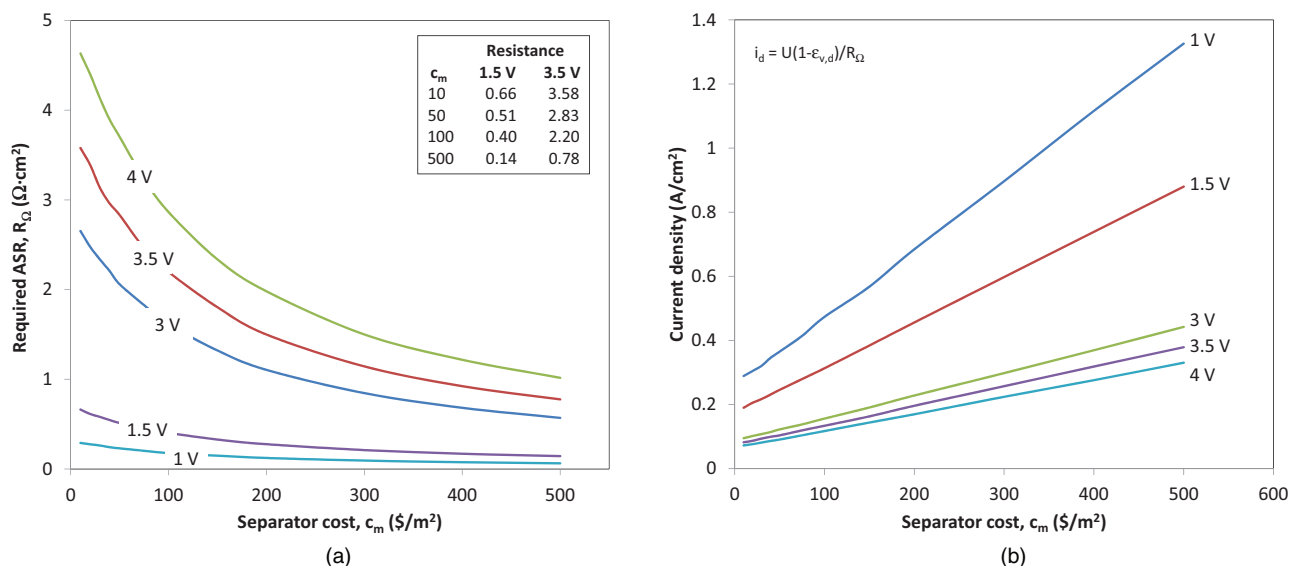| Parameter	Symbol	Minimum	Mode	Maximum	Mean
Reactor cost, $/kWh	p_r	6.0	14.4	21.0	13.8
Nonaqueous OCV, V	U	3	3.5	4	3.5
Aqueous OCV, V	U	1	1.25	1.5	1.25
Separator, $/m^2 (m^2/y)	c_m	16 (10^6)	50 (10^5)	155 (10^4)	74
Flow field, $/m^2	c_{ff}	10	35	55	33
Electrode, $/m^2	c_e	10	30	70	37
Frames and seals, $/m^2	c_s	1	3	6	3.3
Discharge time, h	t_d		5		
System efficiency on discharge	$\varepsilon_{sys,d}$		94%		
Discharge voltage efficiency	$\varepsilon_{v,d}$		91.6%		

Figure 1. Required resistance (a) and current density (b) as a function of separator cost with open-circuit voltage (OCV) as a set parameter. All remaining parameters were sampled from the triangular probability distributions in Table I. OCVs of 1 and 1.5 V represent aqueous RFBs; OCVs of 3, 3.5, and 4 V represent nonaqueous RFBs.

conductivity and thickness for a separator when $R_\Omega = 2.3$ Ω-cm^2. Lines obeying the equation $\kappa = l/R_m$ are shown for $R_m/R_\Omega = 1$ and $R_m/R_\Omega = 0.5$. The optimistic condition $R_m/R_\Omega = 1$ can be approached if the reactions are fast and the electrodes are made of very electronically conductive materials, thereby negating the importance of the conductivities of the electrolytes in the electrodes, and transport losses are minimized by operating at high intra-electrode velocities. The conductivities of lithium-exchanged Nafion 117 (N117) in contact with various organic solvents measured by Doyle et al.[17] are plotted as filled squares at a thickness of 178 μm. Abbreviations

Figure 2. Relationship between conductivity and separator thickness for $R_\Omega = 2.3$ Ω·cm^2. The lines follow the equation $\kappa = l/R_m$. The vertical series labeled Nafion were measured by Doyle et al. for lithium exchanged N117 imbibed with various solvents.[17] Filled squares are data for N117 and open squares are corrected to the thickness of Nafion 211, 25 μm. The vertical series labeled Li-ion are data taken from various literature sources for carbonate electrolytes for lithium-ion batteries. Triangles are bulk values and diamonds are corrected to a porosity of 40%, typical of lithium-ion battery separators. The lithium-ion data is plotted an arbitrary thickness for the sake of presentation and can be moved to the left as appropriate.

are given for the six most conductive solvents: NMF is N-methyl formamide, MeOH is methanol, DMF is N,N′-dimethyl formamide, DMA is dimethylacetamide, DMSO is dimethyl sulfoxide, and NMP is N-methyl-2-pyrrolidone. For comparison, the conductivities of the protonated and lithiated forms of N117 in equilibrium with pure liquid water are 90 and 16.1 mS/cm, respectively.[17] Clearly, Nafion significantly thinner than 178 μm (N117) would be necessary to meet the stipulated ASR with most organic solvents. PEFCs have successfully used ion-exchange membranes that are similar to Nafion and less than 20 μm thick for over a decade. The open squares, which are the aforementioned Nafion conductivities applied to a 25 μm (labeled Nafion 211) membrane, suggest that a small subset of nonaqueous solvents in combination with a thin ion-exchange membrane may be able to achieve the nonaqueous ASR target.

Parasitic transport of active species through the separator inevitably increases as thickness decreases. However, it is reasonable to expect that parasitic crossover will decrease in tandem with conductivity in many cases. That is, solvents that impart detrimental low conductivity may also impart beneficial low crossover. Doyle et al. used pure solvents in all cases. The presence of ions in the bulk solution is anticipated to alter the conductivity of the membrane. For example, Tang et al. showed that bathing N117 in sulfuric acid concentrations below 5 mol/kg enhanced conductivity relative to pure water, while higher concentrations diminished conductivity.[23] The vertical series of data plotted as triangles at an arbitrary thickness consists of the conductivities of various lithium battery electrolytes containing carbonate solvents.[24–26] The rightmost series signified by diamonds at an arbitrary thickness is the data for the Li-ion electrolytes corrected to a porosity of 40% using the formula $\kappa = \kappa_{bulk}\varepsilon^{1.5}$.[27] Commercial Celgard Trilayer separators for Li-ion batteries range from 12 to 38 μm thick.[28] The substantial reduction in conductivity that occurs when an electrolyte is confined within a porous medium brings the conductivities in line with the best combinations of solvent plus Nafion. An ion-exchange membrane like Nafion may inhibit crossover of active species more than a conventional porous separator, which should be weighed against any conductivity differences.

Coulombic efficiency and capacity loss.— Undesired movement of active species through the separator to the opposing electrode is difficult to avoid in flow batteries. The need to minimize crossover depends, in part, upon what happens to active molecules at the counter electrode. At worst, active species may deposit on the surface of the
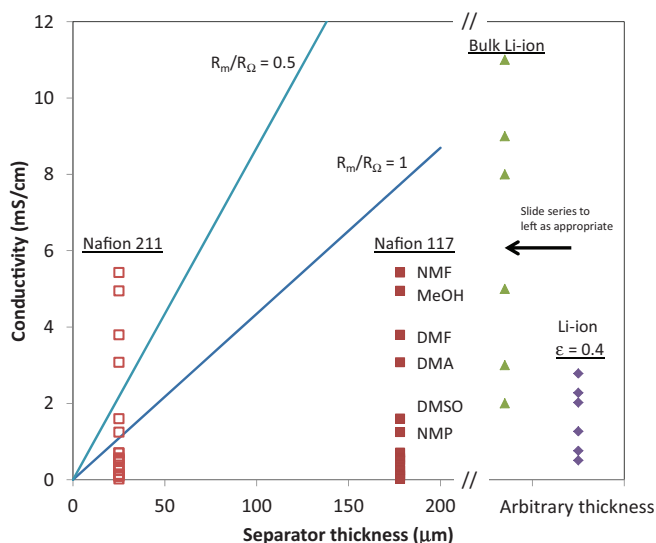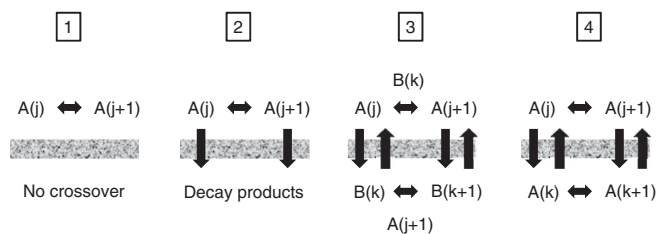
Figure 3. Schematic depiction of the four illustrative cases used to examine the link between Coulombic inefficiency and capacity decline.

electrode becoming unavailable for energy storage and interfering with other essential processes. At best, the active species may be converted to species that participate effectively in energy storage at the invaded electrode. This best scenario describes aqueous vanadium redox batteries. In the worst case, separators or active molecules must be engineered to severely restrict crossover while maintaining high ionic conductivity. Alternatively, if active species that cross the separator retain the ability to store energy then it may be possible to use simple porous materials that allow substantial crossover and employ a scheme to return material to its origin (i.e. balance the electrolyte) periodically provided the attendant Coulombic inefficiency can be tolerated.

The energy efficiency of the reactor in a flow battery is the product of voltage and Coulombic or faradaic efficiencies. The EE of the reactor is multiplied by the efficiency of the system in order to calculate the overall efficiency of the battery. This portion of the analysis focuses on Coulombic inefficiency caused by passage of active species through the separator and assumes that shunt currents, electrical shorts, and side reactions like the formation of passive films and gas evolution can be neglected. The unwanted movement of active species through the separator also causes capacity to decline as the system is cycled. This second effect necessitates increasing the amount, and consequently cost, of active material stored within the system and leads to time-varying performance. The permissible flux through the separator can be set by either efficiency or capacity loss considerations. Energy efficiency is the dominant concern when crossover of the limiting reactant and capacity decline are weakly coupled, while capacity decline is dominant when the coupling is strong.

Coulombic inefficiency and capacity loss are linked because both depend on transport of active redox molecules across the separator. The goal of the derivations that follow is to understand and place bounds on the proportionality constant Ψ in the equation:

$$\frac{dQ}{dt} = -Ai_x\Psi \qquad [2]$$

that relates capacity decline to crossover current density for the four illustrative cases depicted schematically in Figure 3. In Equation 2, Q is capacity in C (or A·h), t is time in s, A is area in cm², and i_x is crossover current density in A/cm². Both i_x and Ψ may vary over the course of extended cycling as the compositions of the electrolytes change; however these changes should be modest for small changes in capacity. Limits on Ψ are derived assuming that the charged species at the negative electrode is the limiting component. This choice is arbitrary and the development can be revised to accommodate other possibilities if desired, however the bounds on Ψ are robust to this choice. With reference to Figure 3, the letter A identifies the chemical

formula of the active center on the negative side, while the letter B identifies the chemical formula of the active center on the positive side in Case 3. The letter j denotes the lowest oxidation state of A on the negative side, while the letter k denotes the lowest oxidation state of either A (Case 4) or B (Case 3) on the positive side. In Case 4, k > j. Only two oxidation states of A or B are permitted on either side of the separator in this analysis. Though not attempted, extending this study to species that exhibit more than two stable oxidation states at either electrode should be possible and dramatic changes in the nature of the results are not expected. Briefly, no crossover occurs in Case 1 so that the CE is always 100%, active molecules that cross the separator are destroyed in Case 2, in Case 3 active species that cross the separator survive and are converted to the oxidation state that is stable at the counter electrode, namely A(j+1) at the positive and B(k) at the negative, finally in Case 4 the active species on both sides of the separator are based on the same molecule or element. Case 3 is conceptually similar to an aqueous iron-chrome battery, while Case 4 is similar to an aqueous all-vanadium battery. While other cases may be conceived of, the four cases tracked in this work cover a broad range of behaviors that encompass many battery systems of interest.

Mole balances on the two oxidation states of active center A on the negative side are:

$$\frac{dN_{A(j)}}{dt} = -\frac{I}{F} - AS_{A(j)} \qquad [3]$$

$$\frac{dN_{A(j+1)}}{dt} = \frac{I}{F} - AS_{A(j+1)} \qquad [4]$$

N_i is the amount of species i in the negative electrolyte in moles, t is the time in s, I is the current in A, F is the Faraday constant in C·mol⁻¹, A is the area in cm², and S_i is the rate of disappearance of species i in mol/cm²·s. Table II shows how $S_{A(j)}$ depends on the fluxes of A and B across the separator in the four cases. The fluxes of A(j) and A(j+1) are positive in the direction from negative electrode to positive electrode, while the fluxes of A(k) and A(k+1) and B(k) and B(k+1) are positive in the direction from positive electrode to negative electrode. In Case 3, B(k+1) that crosses the membrane reacts with A(j) to give A(j+1) and B(k) causing a net decrease in $N_{A(j)}$ and a net increase in $N_{A(j+1)}$. Similarly, $n_{A(k)}$ and $n_{A(k+1)}$ cause a net decrease in $N_{A(j)}$ and a net increase in $N_{A(j+1)}$ in Case 4. That is, species crossing from the positive to the negative in Cases 3 and 4 tend to consume the charged species A(j) and produce the discharged species A(j+1) causing the battery to self-discharge. Hence, for fluxes of similar magnitude $S_{A(j)}$ will tend to be larger than $S_{A(j)}$ in Cases 3 and 4. The coefficients multiplying $n_{A(k)}$ and $n_{A(k+1)}$ can be determined by simultaneously balancing moles and oxidation states. Other molecules, like protons and water in aqueous systems, are needed to completely describe the reactions. The self-discharge processes are assumed to proceed without coupling to side reactions that do not involve active species, like oxygen and hydrogen evolution in Cases 3 and 4. The current is a signed quantity that is positive when the battery discharges and negative when the battery charges. $N_{A(j)}$ decreases when the cell discharges, while $N_{A(j+1)}$ increases. The converse occurs when the battery charges. Both equations involve a single electron transfer because the reactants are one oxidation state apart.

The total amount of A on the negative side is found by summing Equations 3 and 4:

$$\frac{dN_{A-}}{dt} = -A\left(S_{A(j)} + S_{A(j+1)}\right) \qquad [5]$$

Table II. Rates of Disappearance.

Case	$S_{A(j)}$	$S_{A(j)} + S_{A(j+1)}$
1	0	0
2	$n_{A(j)}$	$n_{A(j)} + n_{A(j+1)}$
3	$n_{A(j)} + n_{B(k+1)}$	$n_{A(j)} + n_{A(j+1)}$
4	$n_{A(j)} + (k-j-1)n_{A(k)} + (k-j)n_{A(k+1)}$	$n_{A(j)} + n_{A(j+1)} - n_{A(k)} - n_{A(k+1)}$

Table III. Crossover Current Multipliers and Capacity Loss.

Case Description	1 Perfect separation	2 Destructive crossover	3a, 4a	3b, 4b
			3 – Inert spectators, 4 - Common active	
Capacity loss coupling, Ψ	0	2	0.1	
Cycles before recovery	1250	1250	1250	50
Allowable capacity loss (%)		20%		
Relative charge time, t_c/t_d		2		
Coulombic inefficiency, $1-\varepsilon_{q,rt}$	0	8.1×10^{-5}	0.0016	0.038
Normalized crossover current, i_x/i_d	0	2.7×10^{-5}	5.3×10^{-4}	0.013
i_x/i_d at $\varepsilon_{q,rt} = 97\%$		0.01		

The sums of $S_{A(j)}$ and $S_{A(j+1)}$ are provided in the final column of Table II. Because $A(j+1)$ is present on the positive side of the separator in Case 3, $n_{A(j+1)}$ will tend to be suppressed relative to $n_{A(j)}$. Consequently, the net movement of A across the separator, $n_{A(j)} + n_{A(j+1)}$, will tend to be suppressed in Case 3 compared to Case 2. Similarly, the net movement of A from the negative electrode is suppressed in Case 4 by the countervailing movement of $A(k)$ and $A(k+1)$. For fluxes of similar magnitude, Case 2 should suffer the most rapid capacity decline, while zero capacity loss is conceivable for Cases 3 and 4. Case 1 captures an ideal that may be possible to approach with a very selective separator like an ion-conducting ceramic or large active molecules, Case 2 imposes stringent limits on crossover for a device intended to operate for years, Case 3 relies upon excess active material and solvent, while Case 4 retards crossover like Case 3 while requiring less excess material. Because the crossover rates of the various components usually differ in magnitude, batteries described by Cases 3 and 4 may become unbalanced with repeated cycling which may necessitate maintenance procedures.

The crossover current density is defined as:

$$i_x = F \bar{S}_{A(j)} = \phi F \bar{n}_{A(j)} \qquad [6]$$

The overbar denotes averaging over a complete charge/discharge cycle. The crossover current density is related to the CE of the cell and can be regarded as a gross crossover of $A(j)$. The quantity i_x is a combination of fluxes multiplied by the Faraday constant to facilitate comparison with applied current densities. The crossover process may, or may not, involve electron transfer across a solid/liquid interface. For example, active species in all-vanadium redox cells are converted by redox reactions in the electrolyte phase once they cross through the separator.[29] For an all-vanadium RFB, $j = 2$, $k = 4$ and ϕ would equal 4 if all fluxes were equal in magnitude.

The proportionality constant relating crossover current density and capacity decline can be found by manipulating Equations 2, 5, and 6:

$$\Psi = \frac{\bar{S}_{A(j)} + \bar{S}_{A(j+1)}}{\bar{S}_{A(j)}} \qquad [7]$$

Ψ can be regarded as a ratio of net transfer of $A(j)$ plus $A(j+1)$ to gross transfer of the limiting component $A(j)$. Examination of Table II indicates that all flux contributions to $S_{A(j)}$ are positive as are the coefficients $(k-j-1)$ and $(k-j)$ so $S_{A(j)}$ is always positive. The sum $S_{A(j)} + S_{A(j+1)}$ displays more complicated behavior. i_x is 0 by definition in Case 1, and the value of Ψ is irrelevant. In Case 2 $\bar{n}_{A(j+1)}$ is positive and $S_{A(j)} + S_{A(j+1)} > S_{A(j)}$, so $1 < \Psi < 2$. In Case 3, $A(j+1)$ is present on both sides of the separator and $\bar{n}_{A(j+1)}$ can be positive or negative so $0 < \Psi < 2$. A complete examination Case 4 is more difficult because of the additional fluxes. However, it is easy to show that $\Psi = 0$ when $\bar{n}_{A(j)} = \bar{n}_{A(j+1)} = \bar{n}_{A(k)} = \bar{n}_{A(k+1)}$, which conveys the idea that the presence of the same active center on both sides of the separator will tend to minimize capacity loss. The parameter Ψ should lie in the range $0 < \Psi < 2$ for all cases of interest.

The round-trip CE, $\varepsilon_{q,rt}$, of a complete quasi stationary-state cycle can be found by integrating Equation 3 for charging and discharging

half cycles:

$$\varepsilon_{q,rt} = \frac{Q_d}{Q_c} \approx \frac{1 - i_x/i_d}{1 + \tau i_x/i_d}; \quad \tau = \frac{t_c}{t_d} \qquad [8]$$

Here, the phrase stationary state is used to indicate that immediately preceding and following cycles yield essentially identical results and the word quasi is used as a modifier to indicate that slow capacity decay occurring as the battery cycles prevents the attainment of a true stationary state. The inability to obtain a true stationary state imparts error to the approximation represented by Equation 8. Equation 8 can be used to estimate i_x from measured CE and could be modified to allow for different crossover rates on charge and discharge if warranted.

Table III shows required crossover rates for the four cases depicted in Figure 3. Rows 3 through 6 contain input parameters, while subsequent rows contain outputs. The presence of A on both sides of the separator lowers the rate of capacity loss substantially, hence $\Psi = 0.1$ in Cases 3 and 4. However, practicing Case 3 will tend to increase electrolyte costs because it requires more active material, salt, and solvent for the same capacity. Two variants, (a) and (b), are introduced to admit the possibility of recovering active species that cross the separator in Cases 3 and 4. A battery that cycles every weekday for five years executes approximately 1250 cycles, Cases 1, 2, 3a, and 4a. A criterion of 50 cycles was arbitrarily selected for variants 3b and 4b to address the nuisance and expense of returning the active materials to appropriate balance when capacity decay is recoverable. Schemes that continuously balance the electrolytes, albeit with efficiency penalties, are possible.[30] An allowable decline of 20% matches a failure criterion often applied to lithium-ion batteries in automobiles.[31] A battery that discharges in 5 h and cycles once per day can conceivably charge for 19 h. Maximizing the charging time maximizes the VE, but may result in undesirably high crossover losses. A ratio of charge to discharge times of 2 was selected as a compromise that matches our previous work.[9] All of the above inputs are meant to be representative and reasonable, but clearly a thorough economic analysis could be undertaken to discern a more optimal set of parameters. The crossover rates were calculated with a dimensionless form of Equation 2 integrated for constant i_x and Ψ:

$$\frac{i_x}{i_d} = -\frac{\Delta\theta}{(1 + \tau)m\Psi} \qquad [9]$$

All variables on the right are dimensionless. $\Delta\theta$ is the change in the ratio of present to initial discharge capacity which is a negative quantity, τ is the ratio of charge to discharge times, and m is the number of cycles. The total operating time was approximated as $t_d(1 + \tau)m$, which is appropriate for small changes in t_d. This formulation assumes that no crossover occurs when the battery is not operating.

The final three rows of Table III are calculated outputs. The seventh row shows Coulombic inefficiencies (1-CE), while the eighth row shows the normalized crossover current densities, i_x/i_d. Equation 8 is used to translate between CE and i_x/i_d. The last row gives the ratio i_x/i_d needed to achieve a CE of 97%. This provides an upper limit on i_x that becomes operative in Cases 3b and 4b. The acceptable level of crossover is 20X larger in Cases 3a and 4a than in Case 2. Clearly there is a large benefit associated with using an active material
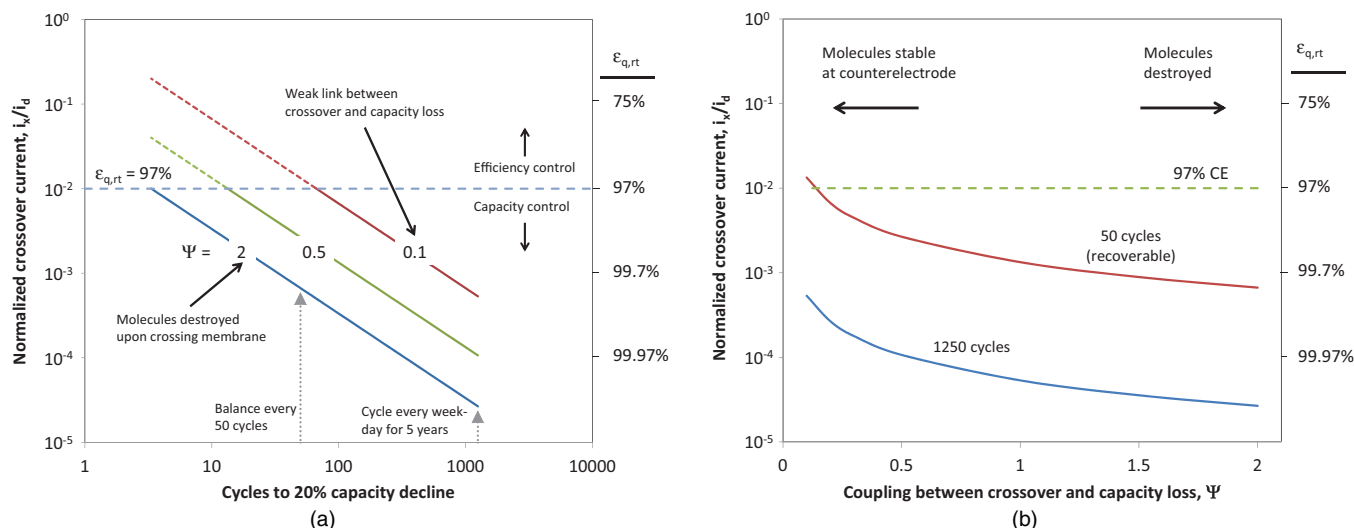
Figure 4. Relationships between capacity decline and i_x (a) and Ψ and i_x (b). $\Psi = 0.1$ represents Cases 3 and 4 where the same active centers are present on both sides of the separator, while $\Psi = 2$ represents Case 2 where reactants are destroyed upon crossing the separator. The ratio $t_c/t_d = 2$.

that is stable at the counter electrode. Furthermore, comparison of variants (a) and (b) shows the substantial relaxation of requirements obtained when periodic balancing of electrolyte is permitted. The ratio i_x/i_d increases by a factor of 25, which equals the ratio of cycle counts. The CE requirement of 97% taken from our previous work[9] is more stringent than the capacity requirement in Cases 3b and 4b with $\Psi = 0.1$.

Figure 4a depicts the relationship between the rate of capacity decline and the characteristic flux of active material across the separator. Curves are shown for three values of Ψ. $\Psi = 0.1$ represents situations where the active molecule is present on the opposite side of the separator as either a spectator or an active participant in the reaction on the opposing electrode, i.e., Cases 3 and 4. Simply put, the net crossover from positive to negative is 90% of the net crossover from negative to positive when $\Psi = 0.1$. $\Psi = 2$ represents situations where active species that cross the membrane are destroyed by reaction, i.e. Case 2. $\bar{n}_{A(j)} = \bar{n}_{A(j+1)}$ when $\Psi = 2$. $\Psi = 0.5$ is an intermediate case. The rate of capacity decline is proportional to Ψ according to Equation 2. The requirements on i_x/i_d are stringent for Case 2 because a large number of cycles must be completed and the multiplier is large. The lines for $\Psi = 0.1$ and 0.5 are dashed when i_x/i_d exceeds the value calculated at $\varepsilon_{q,rt} = 97\%$, which is approximately 0.01. Coulombic efficiency rather than capacity decline is controlling under these circumstances. Figure 4a was constructed assuming constant values of i_x/i_d and Ψ, which is a reasonable first approximation for relatively small capacity changes. The round-trip CE, $\varepsilon_{q,rt}$, is shown on the right vertical axis. Very high efficiencies are necessary to achieve 1250 cycles when Ψ is large. Conversely, when Ψ is small the cycle requirements can be met with larger values of i_x/i_d and the CE target of 97% becomes limiting. Figure 4b phrases the data in Figure 4a differently. The ratio i_x/i_d is plotted as a function of Ψ for 50 and 1250 cycles. The horizontal line at $i_x/i_d \approx 0.01$ corresponds to 97% CE as before.

Evaluation of data from cells.— The parameters R_Ω, i_x, and Ψ can be fit to data obtained with single cells or multi-cell stacks. Allowances must be made for shunt currents when evaluating stack data. Figure 5 illustrates the Coulombic, voltage, and energy efficiencies of a small vanadium redox cell subjected to constant current cycling between 0.7 and 1.65 V. Both electrolytes contained 1.5 M vanadium and 4.1 M total sulfate. The cell had interdigitated flow fields, electrodes consisting of heat treated carbon papers, and a Nafion 212 membrane (NR212).[32] The DC resistance of the cell before testing was >10 kΩ, indicating an absence of electrical shorts. The charge and discharge currents were always equal in magnitude and the data was taken from

the second of two runs done at each condition. The symbols are measured values, while the lines are the curve fits described below. The CE was fit to the formula $\varepsilon_{q,rt} = (i - i_x)/(i + i_x)$ with a best value of i_x of 1.7 mA/cm^2. The VE was fit to the equation $\varepsilon_{v,rt} = (U - i_d R_\Omega)/(U + i_c R_\Omega)$. The best value of R_Ω/U was 0.421 cm^2/A. The average OCV was determined separately to be U = 1.416 V which gives $R_\Omega = 0.596$ m$\Omega \cdot$cm^2. Kinetic losses lead to higher ASRs at low current densities and cause the deviation between model and experiment below 50 mA/cm^2. This cell operates at 200 mA/cm^2 at $\varepsilon_{v,d} = 91.6\%$ hence $i_x/i_d = 0.0085$ and $\varepsilon_{q,rt} = 98.3\%$ when $\tau = 1$. The normalized capacity of the cell during repeated cycling at 150 mA/cm^2 is plotted against the right ordinate. Time in hours was divided by 100 to enable representation of the data with the same abscissa as the efficiencies. The dimensionless capacities cover the range $0.8 < \theta < 1$. Fitting the data gives $|dq/dt| = 0.50$ mA cm^{-2} near maximum capacity, which can be divided by $i_x = 1.7$ mA/cm^2 to yield $\Psi = 0.3$ which is reasonably small as expected for a vanadium redox battery.

Flux.— The previous section addressed the fluxes of active species across the separator that can be tolerated in different circumstances.
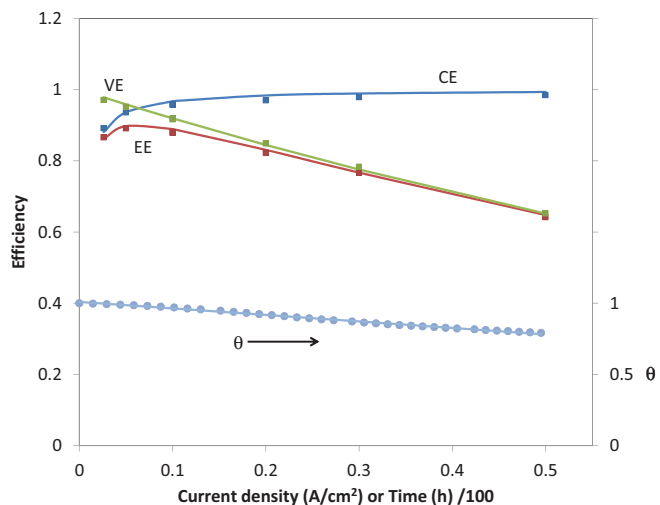

Figure 5. Fits to CE, VE, and EE for a vanadium RFB with a NR212 membrane. Normalized capacity during cycling is plotted against the right vertical axis.

This section examines the terms that contribute to these fluxes. Dilute-solution theory is used to describe transport of active species through the separator by diffusion, migration, and convection (see chapter 11 in Reference 27):

$$n_i = -D_i \nabla c_i - z_i u_i F c_i \nabla \Phi + c_i v \qquad [10]$$

The subscript i identifies the component. n_i is flux in mol/cm$^2 \cdot$ s, D_i is the diffusion coefficient in cm^2/s, c_i is concentration in mol/cm^3, u_i is mobility in cm$^2 \cdot$ mol/J $\cdot$ s, F is the Faraday constant in C/mol e$^-$, Φ is the potential in V, and v is the bulk velocity in cm/s. The bulk velocity is assumed to be equal to the solvent velocity, v_0. Invoking the Nernst-Einstein equation, $u_i = D_i/RT$ where R is the universal gas constant and T is absolute temperature, eliminates the mobility and reduces the number of transport properties in Equation 10. Application of Equation 10 to solutions of high ionic strength, such as those encountered in most batteries, is approximate because it does not address all of the interactions present. Nevertheless, dilute-solution theory is commonly used because it is simple to apply and provides a sound basis for understanding many crucial behaviors.

The importance of the concentration is emphasized by its appearance in all of the flux terms. Concentrations are continuous at the boundaries between simple porous components. By contrast, the concentrations on either side of an interface between an ion-exchange membrane like Nafion and an adjacent bulk solution usually differ. An ion-exchange membrane tends to reject co-ions and accept different counter-ions at ratios that are dissimilar from those that prevail in the contacting bulk solutions. Steric effects become important when the sizes of separator pores and solvated molecules are similar. Thus, it is reasonable to expect that active species, especially large counter-ions, will be less concentrated in an ion-exchange membrane than in a simple separator in contact with the same bulk solution. As a first approximation, we assume that the major charge carriers obey Ohm's law and that the active species contribute negligibly to the conductivity of the membrane. This allows further simplification of Equation 10 with the substitution: $d\Phi/dx \approx -i/\kappa$.

Diffusion and migration of active species.—We begin our analysis by setting $v_0 = 0$ and focusing on the combined effects of diffusion and migration. The flux of A(j) from negative to positive through the membrane divided by the corresponding diffusive component of the flux is (see Appendix A):

$$\frac{n_{A(j)}}{n_{A(j),diff}} = \frac{\beta(e^\beta - \varphi)}{(e^\beta - 1)(1 - \varphi)}; \qquad [11]$$

$$\beta = \frac{zFiL}{\kappa RT} = \frac{zFU(1 - \varepsilon_{v,d})R_m}{RT R_\Omega}; \quad \varphi = \frac{c_2}{c_1}$$

c_1 is the concentration on the negative feed side of the separator, and c_2 is the concentration on the opposite side which is zero for A(j) in all cases. This equation can be applied to a galvanostatic half cycle to good approximation by using the average values of c_1 and c_2. The dimensionless number β is indicative of the relative importance of migration and diffusion. The parameters needed to define β are: valence z, Faraday constant F, current density i, separator conductivity κ, universal gas constant R, and absolute temperature T. The second equality uses a linear polarization equation to replace the current density. The relative importance of migration tends to increase with increasing OCV at fixed VE and with an increasing ratio of membrane to total resistance. Recall that the current is a signed quantity that is positive when the battery is discharging and negative when the battery is charging. Equation 11 is unbounded when $\beta > 0$, but subject to a minimum of zero when $\beta < 0$. Thus, the influence of migration is not symmetric.

Figure 6 shows the normalized fluxes when diffusion and migration tend to move A(j) in the same direction, labelled allied, and when migration opposes diffusion, labelled opposing. $c_2/c_1 = 0$ was assumed in both cases. The linear average of the two fluxes is also shown, labelled average. This describes the net movement over a complete cycle when the current densities during the two half cycles are equal
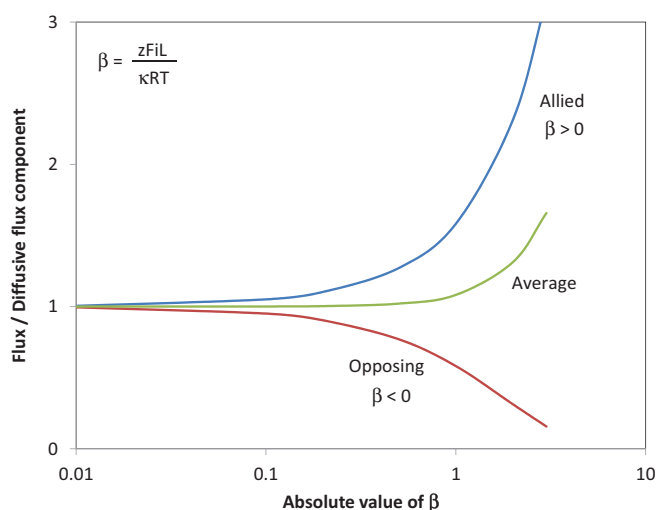

Figure 6. Ratio of total flux to the diffusive component as a function of β. The total flux includes diffusion and migration. The curve labeled allied applies when diffusion and migration drive the active species in the same direction. The curve labeled opposing applies when diffusion and migration drive the active species in opposite directions. The curve labeled average is a linear average of the allied and opposing curves, and describes net movement over a complete cycle for a cell with equal charge and discharge times (and current densities).

in magnitude. As can be seen, the influences of migration during the charging and discharging half cycles do not completely cancel, and there is a net augmentation to diffusion when $\beta > 1$. For U = {1.5, 3, 4}, β_d = {4.9, 9.8, 13.1} $\approx n_{A(j)}/n_{A(j),diff}$, provided $c_2/c_1 = 0$, T = 298.15 K, $\varepsilon_{v,d}$ = 91.6%, z = 1, and R_m/R_Ω = 1. Thus, migration should significantly influence the parasitic movement of active species across the separator in flow batteries operating near target conditions. Furthermore, migration should be more important in non-aqueous batteries because of the higher voltages and lower electrolyte conductivities.

The ratio of the total flux to the diffusive component of the flux averaged over a complete cycle is (see Appendix B):

$$\frac{\bar{n}_{A(j)}}{\bar{n}_{A(j),diff}} = \frac{\beta}{1 + \tau} \left(\frac{1}{1 - e^{-\beta}} - \frac{1}{1 - e^{\beta/\tau}} \right) = g(\beta, \tau) \qquad [12]$$

The overbars denote averaging over a complete charge/discharge cycle. The parameter β, defined in Equation 12, is evaluated for discharging conditions. The parameter τ is a ratio of charge time to discharge time. Figure 7 shows how the ratio of fluxes depends on β and τ. The contribution of migration increases with increasing β and decreases with increasing τ. Diffusion dominates at small β and large τ.

While crossover tests that measure diffusion through separators and membranes for energy-conversion systems such as direct methanol fuel cells,[33] vanadium RFBs,[34] and non-aqueous RFBs[35] are routine, tests that assess migration are relatively rare. Equation 13 relates the diffusive flux to the maximum allowable crossover current density, i_x.

$$n_{A(j),diff} = \frac{D_{A(j)}c_{A(j)}}{l} < \frac{i_x}{\phi F g(\beta, \tau)} \qquad [13]$$

Equation 13 can be used to link ex-situ diffusion measurements to in-situ crossover, thereby negating the need to execute a series of experiments to study the effect of current density on crossover. An all-vanadium flow battery provides a concrete example of how to apply this criterion. Representative performance parameters, U, R_Ω, i_x, Ψ, and i_d, were provided in connection with Figure 5. The ratio R_m/R_Ω is 0.16 assuming a 50.8 μm thick Nafion membrane with a conductivity of 52 mS/cm.[36] β = 1.52 was computed for this set of parameters with z_i = 2 which gives $n_{A(j)}/n_{A(j),diff}$ = 1.09 for τ = 2.
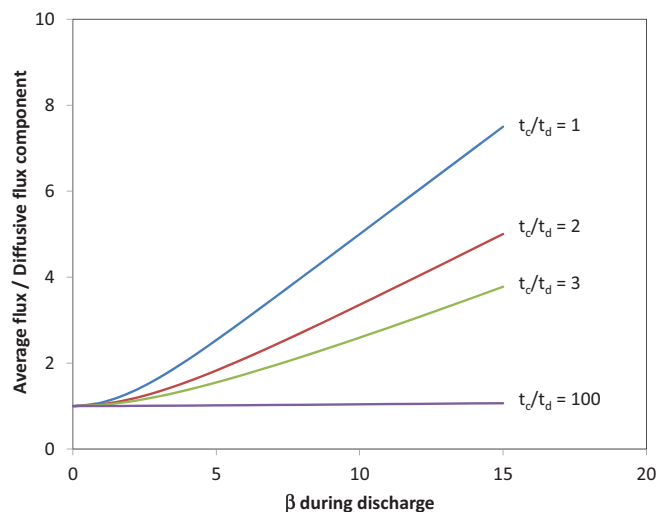
Figure 7. Ratio of total flux to the diffusive flux component averaged over a complete cycle as a function of β during charge for various ratios of charge to discharge time.

Thus, the product $D_i c_i$ measured during a crossover experiment should be less than 2.1×10^{-11} mol/cm·s if $\phi = 4$ (Case 4, j = 2, k = 4 and all fluxes are equal). Examination of results presented by You et al. returns $D_{V4} c_{V4} = 6.8 \times 10^{-11}$ mol/cm·s for VO^{2+} (V4) through Nafion 115.[29] The discrepancy between the results from the cell and the ex-situ tests probably arises because the membranes received different pretreatments. In this example, migration makes a minor contribution to the flux.

Solvent convection.—The convective portion of the flux of active species i across the separator is the product of concentration and solvent velocity, $c_i v_0$. The concentration of an active component can be much lower in an ion-exchange membrane than it is in the adjacent bulk solution. We estimated $c_{V4,m} = 28$ mmol/L for N117 in contact with an aqueous solution containing 1 mol/L VO^{2+} in 4 mol/L total sulfate from the data of Cho et al.[37] A separator with large, uncharged pores will not display similar partitioning. Solvent velocity depends on activity or concentration gradients, electro-osmotic drag, and hydraulic pressure gradients. The following equation empirically captures these contributions:

$$n_0 = c_0 v_0 = -D_0 \nabla c_0 + \frac{\xi i}{F} - \frac{k c_0}{\mu} \nabla P; \quad n_i = \frac{c_i n_0}{c_0} \quad [14]$$

c_0 is the concentration of the solvent in the separator, D_0 is the diffusion coefficient of the solvent, ξ is the drag coefficient, k is hydraulic permeability in cm^2, μ is solvent viscosity in Pa·s, and P is pressure in Pa. Osmotic drag can be neglected in porous separators with uncharged internal surfaces. The viscosity of a solvent confined within small pores inside a membrane can differ from the bulk viscosity, but we ignore this effect.

Magnitudes of flux terms.—Table IV lists representative properties for a Nafion 212 (NR212) membrane in contact with a typical electrolyte for an aqueous all-vanadium RFB. The electrolyte consists of $VOSO_4$, denoted V4, in sulfuric acid. The diffusion coefficients $D_{V4,m}$ and $D_{0,m}$ were calculated from fluxes and intra-membrane concentrations gathered from disparate literature sources. Thus, $D_{V4,m} \Delta c_{V4,m}$ in row 2 was divided by $c_{V4,m}$ in row 3 to give $D_{V4,m}$ in row 4. The same procedure was used to find $D_{0,m}$. Frequently, diffusion through Nafion is reported in terms of bulk, external concentration or activity differences because measuring the concentration in the membrane is difficult and empirically unnecessary in many situations. The hydraulic permeability of NR212 has been observed to decrease as the ionic strength of the contacting electrolyte increases (see Figure 6 in Reference 38, for example). Presumably this is because NR212 shrinks when exposed to electrolytes with high ionic strength.[39] The final four rows contain bulk electrolyte properties and the permeability of a simple porous separator, k_s, for the sake of comparison to the NR212 values.

Table V compares partial fluxes of V4 (multiplied by the Faraday constant) across NR212 and a hypothetical porous separator constrained to have the same ASR, 102 mΩ·cm². The NR212 is 50.8 μm thick, while the separator is 79 μm thick. The electrolyte consists of 0.75 mol/L V4 (equivalent to 1.5 mol/L vanadium at 50% SOC) in 4.1 mol/L total sulfate to match the experiments reported in Figure 5. The resulting concentration of V4 in NR212 was estimated to be 21 mmol/L by interpolating the measurements of Cho et al.[37] The porous separator was assumed to have a porosity of 40% and the bulk transport properties in Table IV were multiplied by $\varepsilon^{1.5}$ to correct for porosity and tortuosity. The driving forces used to make these estimates are listed in the third column. The flux components, with the exception of drag, are uniformly higher for the separator. The diffusive flux for the separator is 5X larger than for NR212. Roughly the same factor applies for migration, while solvent diffusion is 25X larger and pressure driven flow is 2100X larger. Clearly, the CE will be lower for the separator at the same current density. For example, if diffusion were the only term then a cell with NR212 that achieved 97% CE with τ = 2, would achieve just 86% CE with a porous separator. The rate of capacity decline would increase in a similar fashion.

Migration alternately augments and hinders transfer during charge and discharge, as discussed previously. The ionic strengths of the

Table IV. Transport properties for NR212 in contact with a vanadium RFB electrolyte.

Property	Value	Reference	Comments
$D_{V4} \Delta c_{V4}$	6.8×10^{-11} mol/cm·s	50	$\Delta c_{V4,bulk} = 1$ M in 4 M SO_4^{2-}.
$c_{V4,m}$	28 mmol/L	From 37	Bulk: 1 M V4, 4 M SO_4^{2-}.
$D_{V4,m}$	2.4×10^{-6} cm²/s	Calculated	$D_{V4} \Delta c_{V4} / c_{V4,m}$.
$D_0 \Delta c_0$	1.26×10^{-7} mol/cm·s	51	From their Figure 5.
c_0	23 mol/L	Calculated	Using $\lambda = 22$ for pure H_2O.*
D_0	5.5×10^{-6} cm²/s	Calculated	5×10^{-6} cm²/s in Ref. 52
κ_m	50 mS/cm	36	1 M V4 in 5 M sulfate.
k_m	4.09×10^{-16} cm²	53	Pure water through NR212.
ξ	3	54	For 1 M H_2SO_4.
μ	6.6 mPa·s	47	Bulk $VOSO_4$ in 4.1 M SO_4^{2-}.
$D_{V4,bulk}$	2.2×10^{-6} cm²/s	55	0.01-0.5 M V4 in 3 M H_2SO_4.
$D_{0,bulk}$	2.4×10^{-5} cm²/s	56	2.5 M H_2SO_4.
κ_{bulk}	307	57	Interpolated V4 and V5.
k_s	3.75×10^{-14} cm²	Estimated	For $\varepsilon = 40\%$, $d_p = 30$ nm.

*λ = moles of solvent per mole fixed acid site

Table V. Partial Fluxes for NR212 and a Simple Separator with the same ASR.

| | | | $n_i \cdot F$ (mA/cm²) | |
Flux contribution	Equation	Driving force	NR212, 50.8 µm	Separator, 80.5 µm
Diffusion	$n_i = \frac{D_i \Delta c_i}{l}$	$\Delta c_{V4,bulk} = 0.75$ M, $\Delta c_{V4,NR212} = 21$ mM	1.0	5.1
Migration	$n_i = \frac{z_i F D_i c_i i}{RT\kappa}$	$i = 200$ mA/cm²	1.5	8.1
Solvent diffusion	$n_i = \frac{c_{i,m} D_0 \Delta a_0}{l}$	$\Delta a_0 = 0.1$	0.22	5.6
Drag	$n_i = \frac{c_{i,m} \xi i}{c_0 F}$	$i = 200$ mA/cm²	0.55	0
Pressure	$n_i = \frac{c_{i,m} k \Delta P}{\mu l}$	$\Delta P = 10$ kPa	2.5×10^{-4}	0.52

electrolytes, and consequently the solvent activities, on either side of the separator continuously change as the battery charges and discharges because the different oxidation states of the active species have different valences. Consequently, the direction of solvent diffusion is difficult to predict in a general way and varies during cycling. Eventually the battery should reach a pseudo-stationary state where significant variations occur within a cycle, but variations between consecutive cycles are relatively small. Pressure-driven flow appears to be a secondary effect for a hydraulically-impermeable membrane like Nafion. The pressure difference would have to be ~10 MPa in order to bring the magnitude of convection to the level of diffusion and drag. Drag, like migration, acts in opposite directions during charge and discharge. The migration and drag terms are both proportional to current density and independent of membrane thickness. An important distinction between these terms is that migration can be estimated from the product $D_i c_i$, while $c_{i,m}$ is needed in isolation in order to assess drag. The former quantity is more easily measured and more widely reported. The diminution in concentration of active species from bulk to membrane that occurs for NR212 substantially moderates the magnitudes of all of the terms. This moderation disappears for simple separators with large pores, and substantially larger fluxes are predicted.

The treatment of diffusion and convection discussed earlier can be expanded to include electro-osmosis by expanding the definition of β to:

$$\beta = \left(\frac{z_i F}{\kappa RT} + \frac{\xi}{D_i c_0 F} \right) il \qquad [15]$$

Equation 15 applies when solvent diffusion and pressure driven flow can be ignored. Migration and electro-osmosis can either reinforce or cancel each other depending on the valence of the reactant, z_i.

Pore size and pressure driven flow.— The range of hydraulic permeabilities covered by commercial membranes and separators is quite large. Therefore, the contribution of pressure-driven flow to the flux of active species through the separator can vary by orders of magnitude for practical materials. Table VI classifies filtration membranes by pore size. Materials with large hydraulic permeabilities are expected to be unsuitable for flow batteries, because a small pressure difference between the two flowing electrolytes will lead to a large unwanted flow of material. In order to examine this phenomenon, a simple pseudo three-dimensional capillaric model, $k = \varepsilon d_p^2/96$, was

assumed to adequately describe the relationship among pore diameter d_p, porosity ε, and permeability k.[40]

Figure 8 relates pore diameter to flux across a 79 µm separator for different pressure differences subject to the conditions listed in the plot. A simple separator that does not partition the electrolyte was assumed, consequently $c_{i,V4} = 0.75$ M. The total pressure drop experienced by either electrolyte from inlet to exit in a stack will likely be between 10 and 1000 kPa. The pressure difference across the membrane should be no more than 10% of this number, which is the rationale for the values of ΔP in Figure 8. Fitting the permeability in Table IV to the capillaric model gives a pore diameter of 3.1 nm for Nafion assuming a porosity of 40%. This gives $n_{V4}F = 6$ µA/cm² for a 10 kPa pressure difference, which is larger than the value reported in Table V because the concentration in the separator is equal to the bulk concentration of 0.75 mol/L, instead of 21 mmol/L. The volume fraction of solvent in Nafion varies with the osmotic pressure of the external solution. For a sulfuric acid solution, $a_0 = 1$ gives λ = 20 and ε = 40%, while $a_0 = 0.8$ gives λ = 13 and ε = 30%.[23] Thus, resistance to solvent transport through the membrane should increase as the ionic strengths in the adjacent bulk solutions increase. The pores in a typical lithium-ion battery separator are ~30 nm in diameter, which yields 0.52 mA/cm² at 10 kPa. Clearly, maintaining high CE is more challenging with a separator having large pores.

Concentration in separator.— Pore sizes in the reverse-osmosis (RO) and nanofiltration (NF) range should inhibit transport of large active molecules. Table VII compares V4 diffusion through as-received NR212, a NF membrane (Dow NF Nanofiltration Membrane[41]), and a RO membrane (Dow XLE Reverse Osmosis Membrane[42]). The NF and RO membranes are both polyamide based, and are probably positively charged at low pH.[43] The fluxes have been multiplied

Table VI. Properties of Different Classes of Membranes.

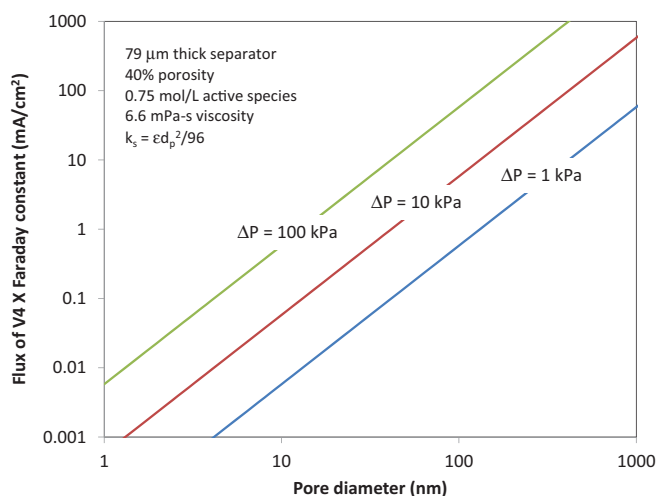| Filtration	Pore size (nm)	Molecular weight cut off (g/mol)
Reverse osmosis (RO)	0.1	100
Nanofiltration (NF)	1	200
Ultrafiltration (UF)	3	2000
Microfiltration	100	200,000
Particle filtration	1000	N/A

Figure 8. Flux across a separator as a function of pore diameter for various pressure differences.

Table VII. Fluxes of V4 through various separators.

	Molecular weight cut off (g/mol)	Barrier thickness (μm)	Pore radius (nm)	V4 diffusion (μA/cm^2)
NR212 (untreated)	-	50.8	1.6	72
Dow Nanofiltration NF	$150-300$[58]	<0.1[59]	0.36 and 0.78[58]	0.12
Dow Reverse Osmosis XLE	100[58]	<0.2[60]	0.42[60]	0.008

by the Faraday constant to facilitate comparison with applied current densities. The fluxes through the NF and RO membranes are considerably lower than the flux through NR212, indicating that separators with small pores may be promising for preventing transport of active molecules. Zhang et al. examined the performances of vanadium RFBs with three NF membranes and discussed the proton and VO^{2+} transport characteristics of the different materials,[44] They observed promising performance in small cells, although they did not provide a comparison to an ion-exchange membrane like Nafion. The flux of V4 through NR212 in Table V is 14X larger than the value in Table VII because the membranes in Table VII were not treated before testing and the pores were shrunken.

Steric hindrance plays an important role when the ratio of molecular radius to pore radius is near 1. Convection of a solute through a separator can be characterized by a reflection coefficient. A reflection coefficient of 1 implies that the membrane completely rejects the solute, while a reflection coefficient of 0 implies that the solute freely moves through the membrane. The steric hindrance pore model relates the reflection coefficient to the ratio of solute radius to pore radius:[45,46]

$$\sigma = 1 - \left(1 + \frac{16r_s^2}{9r_p^2}\right)\left(1 - \frac{r_s}{r_p}\right)^2\left(2 - \left(1 - \frac{r_s}{r_p}\right)^2\right) \quad [16]$$

σ is the reflection coefficient, r_s is the solute radius, and r_p is the pore radius. σ is a monotonically increasing function of r_s/r_p that approaches 0 when r_s/r_p is small and 1 when r_s/r_p approaches 1. Oriji et al. reported a Stoke's radius of approximately 0.3 nm for V4 in concentrated sulfuric acid,[47] which gives $\sigma = 0.70$ for the RO membrane in Table VII. The effective ionic radius of H_3O^+ is approximately 0.1 nm.[48] A separator designed to block V4, $r_p = 0.3$, will have a reflection coefficient near 0.17 for H_3O^+. Thus, the main charge carriers and the active materials need to significantly differ in size in order to use steric hindrance to prevent crossover. The shrinking of the membrane that occurs when it is exposed to high ionic strength should influence steric hindrance.

The presence of fixed charges in a membrane is another factor that affects the concentration and crossover of active molecules. A membrane with negatively charged fixed sites, like Nafion, will tend to reject negatively charged species. An expression for Donnan equilibrium can be used as a first approximation to estimate the ratio of co-ions in the membrane to co-ions in the bulk:[49]

$$K = \frac{c_{-,m}}{c_{-,b}} = \left(\frac{-z_+ c_{+,b}}{z_- c_{-,m} + z_f c_f}\right)^{-z_-/z_+} \quad [17]$$

c_f is the concentration of fixed acid sites in the membrane and z_f is the valence of the fixed sites. The subscripts $+$ and $-$ refer to cations and anions, respectively. This formulation applies when all activity coefficients are 1.

Figure 9 shows the co-ion concentration in the membrane divided by the co-ion concentration in the bulk for a 1:1 salt when $c_f = 1$ mol/L and $z_f = -1$. The tendency for the membrane to reject anions quickly declines as the concentration of ions in the external solution surpasses the concentration of fixed acid sites in the membrane according to
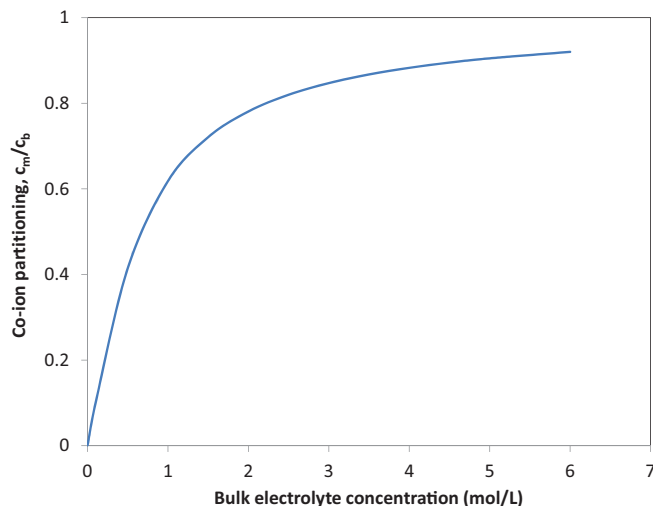

Figure 9. Equilibrium concentration of anions in a cation exchange membrane as a function of bulk electrolyte concentration. Calculated from Donnan equilibrium for a 1:1 electrolyte in a membrane with fixed sites at a concentration 1 M and with a valence of -1.

Figure 9. Electrolytes in flow batteries tend to be highly concentrated which implies that charge exclusion may be relatively weak. This prediction is crude because the electrolytes are assumed to be ideal, although they are highly concentrated.

Conclusions

Transport properties aligned with an aggressive capital cost target of $120/kWh were derived for separators for both aqueous and nonaqueous redox flow batteries. ASR targets of 0.29 and 2.3 $\Omega \cdot$ cm^2 were determined using a Monte-Carlo model with a mean separator price of 74 $/m^2 for aqueous, 1.25 V, and nonaqueous, 3.5 V, batteries. These ASR targets translate to continuous current densities of 360 and 130 mA/cm^2. The required power density decreases when less expensive separators are used. Parasitic crossover, i_x, through the separator affects both Coulombic efficiency and capacity loss. The parameter Ψ was introduced to describe this coupling. Strong coupling between Coulombic inefficiency and capacity decline leads to $\Psi \approx 2$, which necessitates $i_x/i_d \approx 2.7 \times 10^{-5}$ or CE 99.992% to achieve 1250 cycles with 20% capacity decline. The upper limit on $i_x/i_d \approx 10^{-2}$ is controlled by the minimum CE of 97% and is operative when coupling is weak, $\Psi \approx 0$. Achieving low crossover currents may be possible by utilizing separators with small pores that impede pressure driven flow and decrease mobility of active species while allowing for conduction of desired ionic species. Initial estimations suggest these pores should be in the reverse-osmosis or nanofiltration size range.

Acknowledgments

Appendix A

The following equation describes diffusion and migration of a minor component in a dilute solution where the supporting charge carriers follow Ohm's law:

$$n_i = -D_i \frac{dc_i}{dx} + \frac{z_i D_i F c_i i}{\kappa RT}; \quad c(x=0) = c_{i,0}; \quad c(x=l) = c_{i,l} \quad [A1]$$

The following dimensionless variables are defined to simplify notation: $z = x/l$, $\varphi = c_i/c_{i,0}$, $f = n_i l/D_i c_{i,0}$, and $\beta = \frac{z_i F i l}{\kappa RT}$. Substitution yields the dimensionless first-order differential equation:

$$f = -\frac{d\varphi}{dz} + \beta\varphi \; ; \quad \varphi(z=0) = 1 \; ; \quad \varphi(z=1) = \varphi_1 \qquad [A2]$$

This equation is separable because the flux is constant and can be integrated to give:

$$f = \frac{\beta(e^\beta - \varphi_1)}{e^\beta - 1} \qquad [A3]$$

This equation can be divided by the flux when migration is absent, $f = 1 - \varphi_1$, to give Equation 11.

Appendix B

The instantaneous flux across the separator was derived in Appendix A. When the concentration at the far side of the separator is 0, the dimensionless flux is:

$$\frac{\bar{n}}{n_{diff}} = \frac{\beta}{1 - e^{-\beta}} \qquad [B1]$$

The flux averaged over a full charge-discharge cycle is:

$$\bar{n} = \frac{n_d}{1+\tau} + \frac{n_c\tau}{1+\tau} \; ; \quad \tau = \frac{t_c}{t_d} \qquad [B2]$$

Substituting in for the fluxes gives

$$\bar{n} = \frac{n_{diff}}{1+\tau}\left(\frac{\beta_d}{1 - e^{-\beta_d}} + \tau\frac{\beta_c}{1 - e^{-\beta_c}}\right) \qquad [B3]$$

The values of the parameter β during the charging and discharging half cycles are related as follows:

$$\beta_c = \beta_d\frac{i_c}{i_d} = -\frac{\beta_d}{\tau} \qquad [B4]$$

The negative sign appears because the charging current density is a negative quantity while the discharging current density is a positive quantity. Replacing β_c and rearranging gives:

$$\frac{\bar{n}}{n_{diff}} = \frac{\beta_d}{1+\tau}\left(\frac{1}{1 - e^{-\beta_d}} - \frac{1}{1 - e^{\beta_d/\tau}}\right) \qquad [B5]$$

List of Symbols

A	formula for active chemical
A	area, m^2
c_i	cost per unit area of component i, \$/m^2
d	diameter, nm
D_i	diffusion coefficient of i (in solvent), cm^2/s
F	Faraday constant, C/eq
I	current, A
i	current density, A/cm^2
k	permeability, cm^2
l	thickness, cm
m	number of cycles
N	molar amount, mol
n	molar flux, mol/cm$^2 \cdot$ s
NF	nanofiltration
p_r	reactor cost, \$/kWh
Q	extrinsic capacity, C
q	intrinsic capacity, C/cm^2
r	radius, nm
R	universal gas constant, J mol^{-1} K^{-1}
R_i	area-specific resistance of component i, $\Omega \cdot$ cm^2
S_i	rate of disappearance of i, mol cm^{-2} s^{-1}
t	time, s or h
T	temperature, K
U	theoretical open-circuit potential, V
y	SOC
z	valence

Greek

β	dimensionless ratio relating migration and diffusion
ε	efficiency or porosity
ϕ	dimensionless ratio of species disappearance to flux across membrane
φ	concentration ratio
κ	conductivity, S/cm
λ	moles solvent per mole acid site in Nafion
θ	dimensionless capacity
τ	ratio of charge to discharge times
ξ	drag coefficient
Ψ	coupling between inefficiency and capacity loss

Subscripts

+	positive or cation
−	negative or anion
0	initial
bulk	in bulk medium
c	charge
d	discharge
diff	diffusive
e	electrode
ff	flow field
j	lowest oxidation state on negative side
k	lowest oxidation state on positive side
m	separator or membrane
p	pore
q	Coulombic
r	reactor
rt	round trip
s	frames and seals or solute
sys	system
v	voltage
V4	VO^{2+} or $VOSO_4$
x	crossover

References

1. S. Chu and A. Majumdar, *Nature*, **488**, 294 (2012).
2. DOE, "Grid Energy Storage," Washington D.C., 2013.
3. A. Akhil, G. Huff, A. Currier, B. Kaun, D. Rastler, S. Chen, A. Cotter, D. Bradshaw, and W. Gauntlett, "DOE/EPRI 2013 Electricity Storage Handbook in Collaboration with NRECA," Sandia National Laboratories, Livermore, California 94550, 2013.
4. D. Rastler, "Market Driven Distributed Energy Storage System Requirements for Load Management Applicatios," Electric Power Research Institute, Palo Alto, CA, 2007.
5. Z. Yang, J. Zhang, M. Kintner-Meyer, X. Lu, D. Choi, J. Lemmon, and J. Liu, *Chemical Reviews*, **111**, 3577 (2011).
6. A. Weber, M. Mench, J. Meyers, P. Ross, J. Gostick, and Q. Liu, *Journal of Applied Electrochemistry*, **41**, 1137 (2011).
7. C. de Leon, A. Frias-Ferrer, J. Gonzalez-Garcia, and D. W. F. Santoz, *Journal of Power Sources*, **160**, 716 (2006).
8. M. Skyllas-Kazacos, M. Chakrabarti, S. Hajimolana, F. Mjalli, and M. Saleem, *Journal of the Electrochemical Society*, **158**, R55 (2011).
9. R. M. Darling, K. G. Gallagher, J. A. Kowalski, S. Ha, and F. R. Brushett, *Energy Environ. Sci.*, **7**, 3459 (2014).
10. P. Arora and Z. Zhang, *Chem. Rev.*, **104**, 4419 (2004).
11. C. Minke and T. Turek, *J. Power Sources*, **286**, 247 (2015).
12. B. D. James, J. A. Kalinoski, and K. N. Baum, "Mass Production Cost Estimation for Direct H2 PEM Fuel Cell Systems for Automotive Applications: 2010 Update," Strategic Analysis Inc, Arlington, VA, 2010.
13. B. James and A. Spisak, "Mass Production Cost Estimation of Direct H2 PEM Fuel Cell Systems for Transportation Technologies: 2012 Update," Strategic Analysis Inc, Arlington, VA, 2012.
14. M. Mathias, R. Makharia, H. Gasteiger, J. Conley, T. Fuller, C. Gittleman, S. Kocha, D. Miller, C. Mittelsteadt, X. Tao, S. Yan, and P. Yu, *Electrochemical Society Interface*, **14**, 24 (2005).
15. B. Schwenzer, J. Zhang, S. Kim, L. Li, J. Liu, and Z. Yang, *Chemsuschem*, **4**, 1388 (2011).
16. S.-H. Shin, S.-H. Yun, and S.-H. Moon, *RSC Advances*, **3**, 9095 (2013).
17. M. Doyle, M. E. Lewittes, M. G. Roelofs, S. A. Perusich, and R. E. Lowrey, *Journal of Membrane Science*, **184**, 257 (2001).
18. M. Doyle, M. Lewittes, M. Roelofs, and S. Perusich, *Journal of Physical Chemistry B*, **105**, 9387 (2001).
19. L. Su, R. M. Darling, K. G. Gallagher, W. Xie, J. Thelen, N. Balsara, J. S. Moore, and F. Brushett, *under preparation*.
20. A. Zhu, P. D. Christofides, and Y. Cohen, *Journal of Membrane Science*, **344**, 1 (2009).
21. V. Viswanathan, A. Crawford, D. Stephenson, S. Kim, W. Wang, B. Li, G. Coffey, E. Thomsen, G. Graff, P. Balducci, M. Kintner-Meyer, and V. Sprenkle, *J. Power Sources*, **247**, 1040 (2014).
22. K. T. Cho, P. Albertus, V. Battaglia, A. Kojic, V. Srinivasan, and A. Z. Weber, *Energy Technol.*, **1**, 596 (2013).
23. Z. Tang, R. Svoboda, J. S. Lawton, D. S. Aaron, A. B. Papandrew, and T. A. Zawodzinski, *J. Electrochem. Soc.*, **160**(9), F1040 (2013).

24. K. Xu, *Chemical Reviews*, **104**, 4303 (2004).
25. M. S. Ding and T. R. Jow, *J. Electrochem. Soc.*, **151**, A2007 (2004).
26. G. Pistoia, *J. Electrochem. Soc.*, **118**, 153 (1971).
27. J. S. Newman, Electrochemical Systems, 2ed., Englewood Cliffs, New Jersey: Prentice Hall, 1991, p. 468.
28. "http://www.celgard.com/pdf/library/celgard_product_comparison_10002.pdf," 2009. [Online]. [Accessed 12 3 2015].
29. D. You, H. Zhang, C. Sun, and X. Ma, *Journal of Power Sources*, **196**, 1578 (2011).
30. L. Mou, M. Huang, A. Klassen, and M. A. M. Harper, "Redox flow battery and method for continually operating the redox flow battery for a long time." Pat. EP2339682 A1, 29 June 2011.
31. J. Neubauer, A. Pesaran, C. Bae, R. Elder, and B. Cunningham, *Journal of Power Sources*, **271**, 614 (2014).
32. R. M. Darling and M. L. Perry, *J. Electrochem. Soc*, **161**(9), A1381 (2014).
33. A. Heinzel and V. M. Barragan, *Journal of Power Sources*, **84**, 70 (1999).
34. Z. Mai, H. Zhang, X. Li, C. Bi, and H. Dai, *Journal of Power Sources*, **196**, 482 (2011).
35. S. Shin, S. Yun, and S. Moon, *RSC Adv*., **3** 9095 (2013).
36. Z. Tang, R. E. Keith, D. S. Aaron, J. S. Lawton, A. B. Papandrew, and T. A. Zawodzinski, *ECS Transactions*, **41**(23), 25 (2012).
37. H. Cho, M. Ohashi, and J. W. Van Zee, *J. Power Sources*, **267**, 547 (2014).
38. A. Narebska, S. Koter, and W. Kujawski, *Journal of Membrane Science*, **25**, 153 (1985).
39. A. Kusoglu, K. T. Cho, R. A. Prato, and A. Z. Weber, *Solid State Ionics*, **252**, 68 (2013).
40. F. A. L. Dullien, Porous Media Fluid Transport and Pore Structure, 2 ed., San Diego, Ca: Elsevier Science, 1992, 260.
41. Sterlitech Corporation, [Online]. Available: http://www.sterlitech.com/membrane-process-development/flat-sheet-membranes/nanofiltration-nf-membrane/nanofiltration-nf-membrane-ymnf3001.html. [Accessed 14 April 2015].
42. Sterlitech Corporation, [Online]. Available: http://www.sterlitech.com/membrane-process-development/flat-sheet-membranes/reverse-osmosis-ro-membrane/reverse-osmosis-ro-membrane-ymxle3001.html. [Accessed 14 April 2015].
43. A. E. Childress and M. Elimelech, *Journal of Membrane Science*, **119**, 253 (1996).
44. H. Zhang, H. Zhang, X. Li, Z. Mai, and J. Zhang, *Energy Environ. Sci.*, **4**, 1676 (2011).
45. X. L. Wang, T. Tsuru, M. Togoh, S. Nakao, and S. Kimura, *J. Chem. Eng. Jpn.*, **28**, 186 (1995).
46. J. Schaep, B. Van der Bruggen, C. Vandecasteele, and D. Wilms, *Separation and Purification Technology*, **14**, 155 (1998).
47. G. Oriji, Y. Katayama, and T. Miura, "*Electrochimica Acta*," **49**, 3091 (2004).
48. Y. Marcus, *The Journal of Chemical Physics*, **137**, 154501 (2012).
49. W. J. Moore, Physical Chemistry, 4 ed., Englewood Cliffs, NJ: Prentice-Hall, Inc., 1972, 544.
50. C. Sun, J. Chen, H. Zhang, X. Han, and Q. Luo, *J. Power Sources*, **195**, 890 (2010).
51. S. Motupally, A. J. Becker, and J. W. Weidner, *Journal of the Electrochemical Society, 2000*, **147**(9), 3171 (September 2000).
52. Q. Zhao, P. Majsztrik, and J. Benziger, *Journal of Physical Chemistry B*, **115**, 2717, 2011.
53. Q. Duan, H. Wang, and J. Benziger, *Journal of Membrane Science*, **392–393**, 88 (2012).
54. B. S. Pivovar, W. H. Smyrl, and E. L. Cussler, *J. Electrochem. Soc.*, **152**(1), A53 (2005).
55. S. Zhong and M. Skyllas-Kazacos, *J. Power Sources*, **39**, 1 (1992).
56. S. Umino and J. Newman, *J. Electrochem. Soc.*, **140**(8), 2217 (August 1993).
57. M. Skyllas-Kazacos and M. Kazacos, *J. Power Sources*, **196**, 8822 (2011).
58. D. Dolar, A. Vukovic, D. Asperger, and K. Kosutic, *Journal of Environmental Sciences*, **23**(8), 1299 (2011).
59. V. Freger, *Environ. Sci. Technol.*, **38**, 3168 (2004).
60. E. Drazevic, K. Kosutic, and V. Freger, *Water Research*, **49**, 444 (2014).